High-frequency tuning of photonic crystal defect cavity modes using surface acoustic waves

D. A. Fuhrmann[a,b], H. Kim[b,c], S. M. Thon[c], J. Jambreck[a], J. Ebbecke[a,d], D. Bouwmeester[c,e], P. M. Petroff[b,f], A. Wixforth[a] and H. J. Krenner[a]

[a]Institut für Physik der Universität Augsburg, Lehrstuhl für Experimentalphysik I, Universitätsstr. 1, 86159 Augsburg, Germany
[b]Materials Department, University of California, Santa Barbara, CA 93106, USA
[c]Physics Department, University of California, Santa Barbara, CA 93106, USA
[d]NanoSYD, University of Southern Denmark, D-6400 Sønderborg Denmark
[e]Huygens Laboratory, Leiden University, P.O. Box 9504, 2300 RA Leiden, The Netherlands
[f]Department of Electrical and Computer Engineering, University of California, Santa Barbara, CA 93106, USA

ABSTRACT

We study the influence of the mechanical deformation induced by a surface acoustic wave (SAW) on the resonance frequency of a defect cavity in a 2D photonic crystal membrane. Using FDTD-simulations we determine the resonance frequency and quality factor of a nanocavity of a GaAs based structure with embedded InAs quantum dots. Under the influence of a SAW, we find a periodic modulation of the cavity resonance wavelength of $\Delta\lambda > 2$ nm accompanied by only a weak $< 0.5\times$ reduction of the Q-factor. Initial experiments for a SAW wavelength of $\sim 1.8\mu$m show a pronounced broadening of the time-integrated cavity emission line corresponding to a shift of ≥ 1 nm.

Keywords: Photonic Crystal Membrane, Surface Acoustic Waves, Nanocavities, Spectral Tuning

1. INTRODUCTION

Optical nanocavities defined in two-dimensional photonic crystal membranes (PCMs) with embedded quantum dots (QDs) have attracted widespread interest since they provide a direct route to implement a cavity-quantum electrodynamic system (cQED) in the solid state.[1,2] Over the last five years, significant progress was made ranging from the observation of weak[3,4] and strong coupling,[5-9] lasers with ultra-low thresholds[10] and on-chip single photon devices.[11]

A key requirement to study such effects or their application for quantum information schemes[12,13] relies on the possibility to tune the QD and the nanocavity wavelengths. Such tunability allows e.g. for the study of dephasing effects and light-matter interaction in the single photon limit.[2,14] A variety of techniques of tuning either the cavity resonance or the emission energy of a quantum dot by exploiting such as the temperature dependence of the refractive index of the material,[5,15] wet chemical etching[16] or by the absorption of inert gas onto the photonic crystal slab at low temperatures[17,18] have been successfully demonstrated. Recently, static electric fields giving rise to the Quantum Confined Stark Effect of the QD were used in an electrically active structure.[9,14] However, the tuning speed of all these approaches is limited and manipulation on the timescales of the processes at play is difficult to achieve.

Here, we demonstrate an alternative route towards real-time control of such structures employing surface acoustic waves (SAWs) which are a periodic deformation of the surface of a material. Using finite-difference time domain simulations (FDTD) we demonstrate that this mechanical deformation by the SAW gives rise to a periodic modulation of the cavity emission wavelength by $\Delta\lambda > 2$ nm without significant degradation of the quality

Further author information:
D. A. Fuhrmann: E-mail: daniel.fuhrmann@physik.uni-augsburg.de
H. J. Krenner: E-Mail: hubert.krenner@physik.uni-augsburg.de

Photonic and Phononic Crystal Materials and Devices X, edited by Ali Adibi, Shawn-Yu Lin, Axel Scherer, Proc. of SPIE Vol. 7609, 760908 · © 2010 SPIE · CCC code: 0277-786X/10/$18 · doi: 10.1117/12.842710

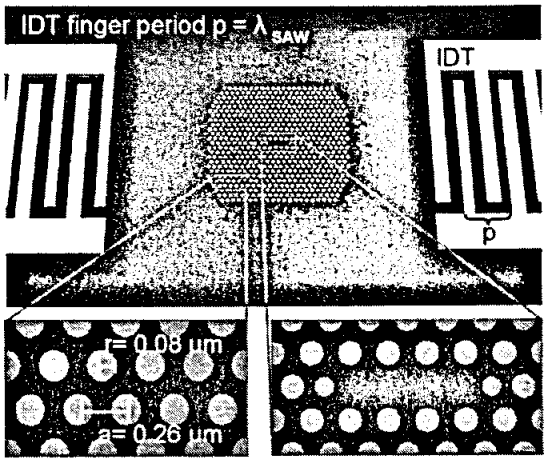

Figure 1. (Color online) Sketch of the sample layout (not to scale): *Upper panel:* A PCM is located between two IDTs which are used to excite a SAW. *Lower panels:* The PCM lattice parameters and the L3 cavity design used for FDTD simulations.

factor. These simulations are supported by proof of principle experiments where in the time-integrated spectra a significant broadening of the cavity emission is observed.

In piezoelectric semiconductors such as GaAs SAWs can be excited over a large wavelength (λ_{SAW}) range from several tens of microns down to ≤ 120 nm[19] with vertical and lateral displacements A_{SAW} of a few nanometers of the surface. Taking into account the SAW phase velocity of $v_{SAW} = 2.87 \cdot 10^5$ cm/s on a (001) GaAs surface in [110] direction this wavelength range corresponds to frequencies of < 100 MHz up ≥ 20 GHz. For one dimensional photonic structures SAW have already been successfully applied by Santos et al.[20] to tune the optical properties.

2. SIMULATION OF OPTICAL PROPERTIES OF A PCM DEFORMED BY A SAW

In this section we present the sample and PCM designs used for FDTD-simulation and calculate the response of the optical properties (cavity wavelength and Q-factor) under SAW mediated deformation.

2.1 Sample design

The simulated PCM sample layout shown in Fig. 1 consists of a triangular lattice of air-holes in a GaAs-matrix (refractive index $n_{matrix} = 3.54$) with a lattice constant $a = 0.26$ μm and air hole radius $r = 0.08$ μm. The resulting air-fill factor is $r/a \approx 0.31$ optimized for a membrane thickness of $d = 130$ nm. In the center of the photonic crystal three holes are missing to form a $L3$-cavity. In order to achieve the maximum Q-factor, holes at the perimeter of the cavity are shifted spatially and their radius was adjusted (see Fig. 1). As can be seen in Fig. 1, interdigital transducers (IDT) are positioned on either side of the PCM. When a radio-frequency (RF) voltage is applied to these comb electrodes, a periodic deformation is induced in a piezoelectric substrate. A SAW can be excited if its frequency f_{RF} matches the dispersion relation $f_{RF} = v_{SAW}/p_{SAW}$. Therefore, the resulting SAW wavelength λ_{SAW} is determined by the periodicity p of the IDT. Furthermore, the SAW propagation is aligned with the long axis of the $L3$ cavity.

2.2 Cavity designs

We perform FDTD-simulation to calculate the variation of the optical properties of the PCM. From the FDTD-simulation we deduce the cavity resonance frequency f_{res} from the fourier transform of the time domain of the electromagnetic components inside the cavity. The Q-factor is determined by the cavity ring-down time, the

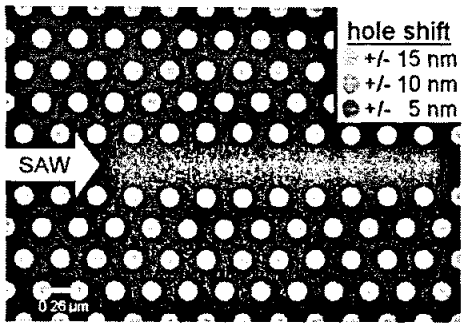

Figure 2. Design of the waveguide nanocavity.

temporal decay of the electromagnetic field envelope.
The main cavity design studied in this paper is the $L3$-cavity presented in Fig. 1. For the unperturbed cavity, we calculate a resonance at $\lambda_{r0} = 957.21$ nm with a Q-factor $Q_0 \approx 67500$ for the fundamental optical mode.

In addition to the $L3$-cavity, we have investigated the effect of SAW on a second type of nanocavity design shown in Fig. 2. The lattice parameter a is chosen to be the same as for the $L3$-cavity, whereas $r = 0.067\mu m$. This type of cavity (WG-cavity) is based on a PCM waveguide with local width modulation[21] as indicated in Fig. 2. By shifting the position of a set of holes highlighted in the figure, a local optical confinement potential is created giving rise to a high-Q optical mode at $\lambda_{0,WG} = 1005.94$ nm.

3. FDTD SIMULATION OF SAW MEDIATED NANOCAVITY TUNING

For FDTD-simulations of this structure, we assume a SAW with a frequency $f_{SAW} > 1.5$ GHz corresponding to a wavelength $\lambda_{SAW} = 1.8\ \mu$m or $\sim 7\times$ the lattice constant (a) of the PCM. Since this frequency and timescale is longer than typical radiative lifetimes of QDs weakly or strongly coupled to a cavity mode (< 200 ps[4,6]) we can treat the SAW driven deformation as a quasi-static perturbation.

In a first step, we computed the lateral deformation of the PCM as a function of the local SAW phase (ϕ_{SAW}) at the position of the cavity. For visualization the deformed cavity for $A_{SAW} = 50$ nm* at distinct values of ϕ_{SAW} is shown in Fig. 3: For $\phi_{SAW} = 0$, an antinode is at the cavity center, for $\phi_{SAW} = 1.5\pi$ a node. Clearly, as ϕ_{SAW} changes, two fundamental geometric parameters of the photonic crystal, the lattice constant a and the hole radius r and, hence, the r/a ratio at the cavity oscillates.

3.1 L3-cavity

The calculated emission line of the main cavity resonance for a SAW amplitude $A_{SAW} = 1$ nm is plotted in Fig. 4 for $\phi_{SAW} = 0$, π and 1.5π at which a maximum, a minimum or a node of the SAW is lined up with the cavity position, respectively (see Fig. 3). Clearly, λ_c exhibits a pronounced oscillation with an amplitude of $\Delta\lambda_c \sim 1.5$ nm as ϕ_{SAW} changes. The linewidths of these resonances appear broadened due to the finite time element used in the FDTD simulation. However, we can determine the Q-factors at these values of ϕ_{SAW} from the temporal decay of the electromagnetic field envelope to 78000, 60000 and 88000, respectively. This is comparable to the undeformed cavity.

In order to investigate this effect on the resonance wavelength (λ_c) and the Q-factor in more detail, we vary ϕ_{SAW} between 0 and 2π for $A_{SAW} = 0.5$ nm, 1 nm and 2 nm. The calculated values of λ_c and the Q-factor are

*The large amplitude was chosen in order to visualize the deformation which would not be resolvable for the realistic values of a few nanometers.

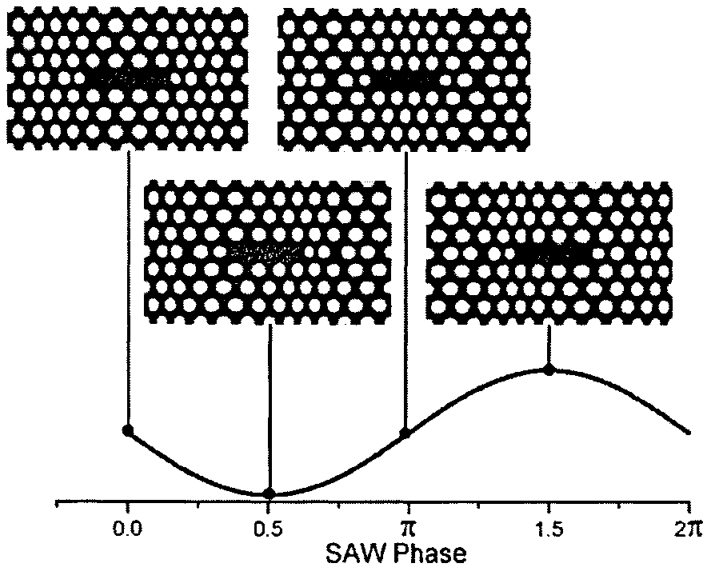

Figure 3. Deformation of the $L3$-cavity for different values of ϕ_{SAW} for $\lambda_{SAW} = 7a$ and $A_{SAW} = 50$ nm. The unusual large value for the SAW amplitude was chosen to visualize the effect in the figure.

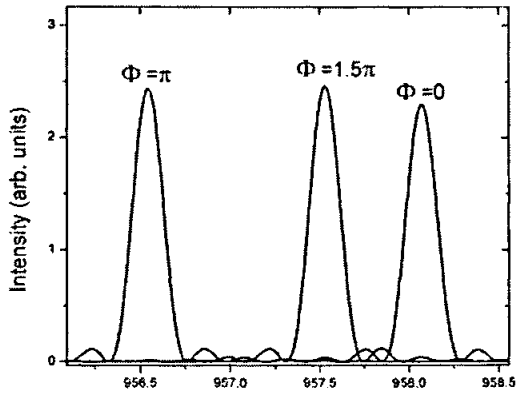

Figure 4. Spectra of the simulated $L3$-cavity resonance for different SAW-phases and $A_{SAW} = 1$ nm.

plotted as symbols in Figs. 5 and 6.
For λ_c, we obtain a sinusoidal variation as ϕ_{SAW} is tuned. The tuning range $\Delta\lambda$ increases linearly from 1 nm to 1.7 nm to 2.6 nm for $A_{SAW} = 0.5$ nm, 1 nm and 2 nm, respectively. The phase dependence of λ_c is well reproduced by the phase dependence of the air-fill factor r/a shown as a solid line in Fig. 5. The deformation of the structure changes both the radius and the shape of the air holes and gives rise to an elongation and compression along the SAW propagation direction. Depending on the local SAW phase, r/a is either reduced or increased which results in a change of the width of the photonic band gap,[4,22] which implies a change of the resonance wavelength. The good agreement of this effect and the calculated spectra shift as a function of ϕ_{SAW} clearly indicates that this geometry effect is indeed the dominant mechanism underlying the cavity tuning.

A crucial requirement for any application of such a tuning mechanism is that the Q-factor remains sufficiently high and is not significantly reduced when compared to the undeformed, optimized cavity. To asses the potential

of our SAW-based tuning method, we analyze the variation of the Q-factor as a function of ϕ_{SAW} relative to Q_0 which is given by

$$\Delta Q(\phi_{SAW}) = \frac{Q(\phi_{SAW}) - Q_0}{Q_0}. \quad (1)$$

In Fig. 6 ΔQ is plotted for the three values of A_{SAW}. Analogous to the shift of λ_c, we also observe an oscillation of ΔQ with ϕ_{SAW} being in phase with the r/a variation. The strongest reduction of the Q-factor of 28 % is found for $A_{SAW} = 2$ nm, sufficiently high for application in tunable cQED experiments. This is further underlined by the fact that from this minimum of the Q-factor, we obtain an overall tuning range of 36, 109 and 130 cavity linewidths for $A_{SAW} = 0.5$ nm, 1 nm and 2 nm. This result proves that our approach is a very effective tuning mechanism. A scale for the linewidth in respect to $\Delta\lambda$ is included in Fig. 5.

A second crucial requirement for optimum coupling between a QD and a nanocavity mode is the spatial alignment of the photon emitter and the maximum of the electric field distribution of the mode.[3,6,8] To confirm that optimum spatial overlap is maintained, we compare the calculated in-plane E-field distributions at $\phi_{SAW} = 0$ and $\phi_{SAW} = \pi$ where the cavity is compressed and expanded by the SAW ($A_{SAW} = 1$ nm), respectively. Since the deformation is symmetric with respect to the center of the cavity, we compare these distributions in one panel. The result for the compressed ($\phi_{SAW} = 0$) and expanded cavity ($\phi_{SAW} = \pi$) are plotted on the left and

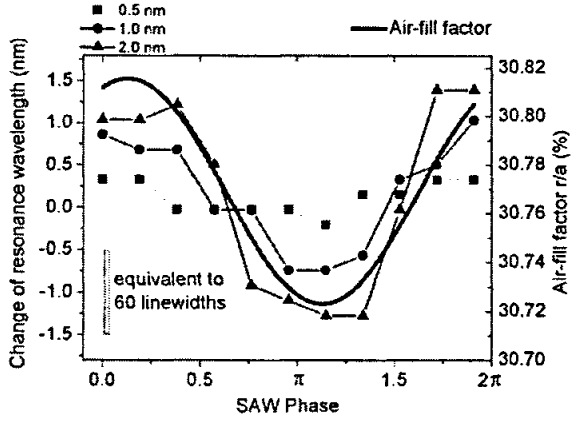

Figure 5. Shift of the cavity resonance ($\Delta\lambda_c$) relative to the undeformed case (symbols) for different values of A_{SAW} and the variation of the air-fill factor (solid line) as a function of ϕ_{SAW}.

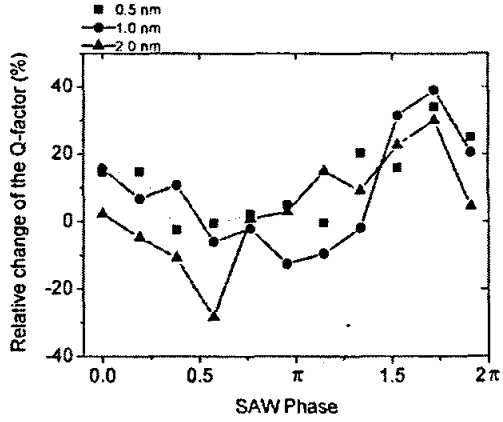

Figure 6. Relative change of the Q-factor as a function of the SAW phase relative to the undisturbed cavity.

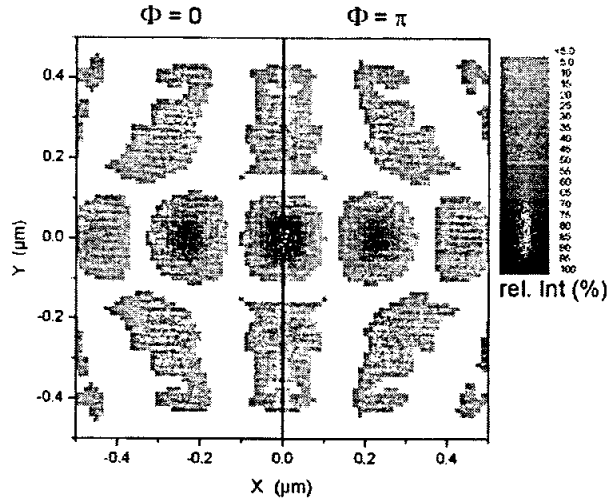

Figure 7. Electric field distributions of the fundamental mode of a $L3$-cavity under compression ($\phi_{SAW} = 0$, left half) and expansion ($\phi_{SAW} = \pi$,right half).

right of Fig. 7. When comparing the two field distributions, we find that no significant variation of the spatial mode distribution occurs at the phases of maximum deformation of the cavity. Thus, this absence of spatial shifts of the anti-nodes of the electric field in the nanocavity ensures that no pronounced effects degrading the cavity-emitter coupling have to be expected.

3.2 Waveguide cavity

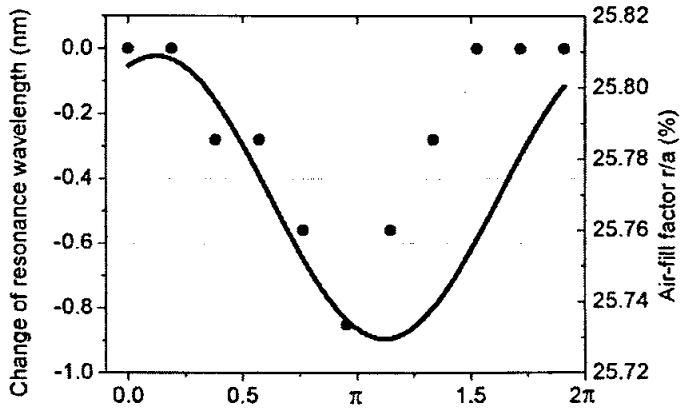

Figure 8. Resonance shift of waveguide cavity as function of the SAW phase.

Similar calculations were preformed for the WG-cavity: For this nanocavity design, we also observe a SAW-driven tuning of the fundamental cavity resonance similar to that of $L3$-cavity. As an example, the spectral shift $\Delta\lambda_c$ as a function of ϕ_{SAW} for a SAW amplitude of $A_{\mathrm{SAW}} = 1$ nm is shown as symbols in Fig. 8. When compared to the $L3$-cavity, these spectral shifts are reduced by $\sim 50\%$ and only occur towards shorter wavelengths. In addition, the geometry dominated phase dependence is preserved (solid line). The reduced tuning range can be understood qualitatively by the fact that this cavity is realized within a one-dimensional waveguide.

4. TIME-INTEGRATED PHOTOLUMINESCENCE

In order to confirm the proposed tuning mechanism, we fabricated samples combining both PCM with embedded self-assembled InAs/GaAs QDs and IDTs for SAW generation. A scanning electron micrograph (SEM) of a typical sample layout is shown in Fig. 9. In the upper part an IDT is positioned which can be used to excite a SAW propagating towards an array of PCM in the lower part.

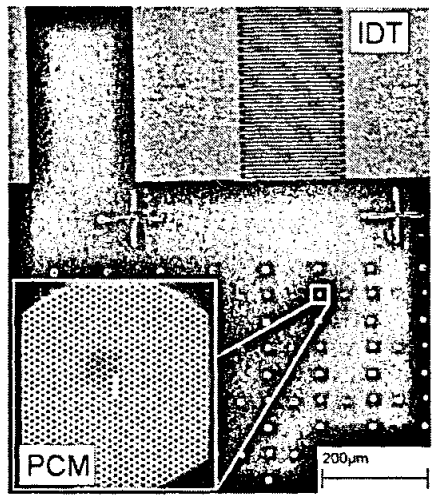

Figure 9. SEM picture of sample consisting of IDTs on the upper part for SAW generation and an array of PCMs on the lower part.

For proof of principle experiments, a similar sample containing IDTs with a design wavelength (λ_{SAW} = 1.8μm) as used in the simulations was studied by conventional *time-integrated* μ-photoluminescence (μ-PL) at low temperatures (T = 5 K). In this experiment, however we are not able to resolve the spectral shift over one SAW period but integrate over all phases. Typical μ-PL spectra taken for different SAW powers (P_{SAW}), i.e. values of A_{SAW} are presented in Fig. 10 (a). For low SAW powers and negligible deformation of the PCM, the unperturbed cavity emission is detected at $\lambda_{c,0}$ = 937.75 nm and a moderate Q-factor of $\sim$ 2000. As the SAW is generated with P_{SAW} = 13 dBm, the cavity emission line begins to broaden. This broadening increases to $\Delta\lambda_c \sim 1$ nm as P_{SAW} is increased to 16 dBm. As pointed out in the beginning of this section, these experiments were performed time-integrated and average over all phases. Therefore, the observed broadening corresponds to the amplitude of the spectral shift due to SAW-tuning and is in good agreement with the calculated values.

To further confirm that this shift arises from a SAW-driven deformation we kept the RF power constant at P_{SAW} = 16 dBm and scanned the frequency. The corresponding μ-PL spectra are shown in Fig. 10 (b) along with a schematic of the frequency response of an IDT as an inset. The periodicity p of the IDT determines the center frequency at which SAWs can be excited which is spectrally broadened. Therefore, the generated SAW power and, also A_{SAW} falls off when the RF frequency is tuned away from the resonance. This anticipated behavior is well reproduced by the experimental data shown in Fig. 10 (b). Here, for a detuning of $<$ 2 MHz away from the IDT resonance at $\sim$ 1639.4 MHz, the broadening disappears. The overall red-shift of the cavity signal with increasing P_{SAW} arises from a weak heating effect by the SAW. This heating can be minimized for pulsed SAW excitation. In our time-integrated experiments, however, SAW pulses would lead to a superposition of the tuning effect and the unperturbed cavity. Due to the enhanced signal of the undeformed cavity a clear discrimination would be difficult. We are presently investigating an alternative timing sequence to overcome this obstacle.

The presented experimental data clearly shows that a SAW can be applied to tune the resonance wavelength of

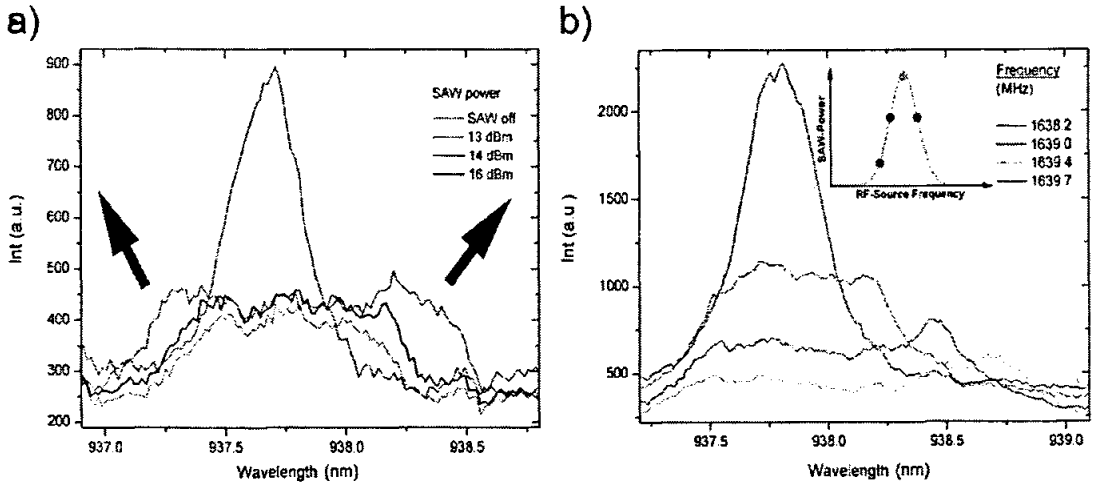

Figure 10. Cavity spectra recorded for different SAW powers (a) and RF frequencies (b).

a PCM nanocavity. The observed value of $\Delta\lambda_c \sim 1\text{nm}$ corresponds to the $A_{SAW} \sim 0.5 - 1\text{nm}$ as expected for a high power SAW.

5. CONCLUSION

Employing FDTD-simulations we have studied the effect of a SAW induced deformation of a two dimensional high-Q PCM on its resonance frequency λ_c and Q-factor. We demonstrated that for an optimized $L3$-cavity and a $A_{SAW} = 2$ nm SAW an overall shift in the resonance wavelength exceeding 130 spectral linewidths can be achieved. This shift follows the phase dependency of r/a and, thus, the geometric change of the PCM. Furthermore, the Q-factor is only weakly decreased by less than 50% and the spatial mode profile is only slightly changed. Therefore, this SAW-based approach could be used for high-frequency tuning of nanocavity modes for cQED experiments. In initial, time-integrated proof of principle experiments averaging over many SAW periods, we were able to demonstrate that the emission of a $L3$-cavity is broadened by the investigated SAW-based tuning mechanism.

ACKNOWLEDGMENTS

This work was supported in part by the German federal government under the Cluster of Excellence *Nanosystems Initiative Munich* (NIM). A portion of this work was done in the UCSB nanofabrication facility, part of the NSF funded NNIN network. One of us (D. A.F.) acknowledges financial support by the Bayerische Forschungsstiftung.

REFERENCES

1. S. Noda, M. Fujita, and T. Asano, "Spontaneous-emission control by photonic crystals and nanocavities," *Nature Photonics* **1**, pp. 449–458, August 2007.
2. I. Fushman, D. Englund, A. Faraon, N. Stoltz, P. Petroff, and J. Vučković, "Controlled Phase Shifts with a Single Quantum Dot," *Science* **320**, pp. 769–772, May 2008.
3. A. Badolato, K. Hennessy, M. Atatüre, J. Dreiser, E. Hu, P. M. Petroff, and A. Imamoglu, "Deterministic coupling of single quantum dots to single nanocavity modes," *Science* **308**, pp. 1158–1161, 2005.
4. A. Kress, F. Hofbauer, N. Reinelt, M. Kaniber, H. J. Krenner, R. Meyer, G. Böhm, and J. J. Finley, "Manipulation of the spontaneous emission dynamics of quantum dots in two-dimensional photonic crystals," *Physical Review B* **71**, p. 241304, Jun 2005.

5. T. Yoshie, A. Scherer, J. Hendrickson, G. Khitrova, H. M. Gibbs, G. Rupper, C. Ell, O. B. Shchekin, and D. G. Deppe, "Vacuum rabi splitting with a single quantum dot in a photonic crystal nanocavity," *Nature (London)* **432**, pp. 200–203, 2004.
6. K. Hennessy, A. Badolato, M. Winger, D. Gerace, M. Atatüre, S. Gulde, S. Fält, E. L. Hu, and A. Imamoğlu, "Quantum nature of a strongly coupled single quantum dot-cavity system," *Nature (London)* **445**, pp. 896–899, Feb. 2007.
7. D. Englund, A. Faraon, I. Fushman, N. Stoltz, P. Petroff, and J. Vuckovic, "Controlling cavity reflectivity with a single quantum dot," *Nature (London)* **450**, pp. 857–861, Dec. 2007.
8. S. M. Thon, M. T. Rakher, H. Kim, J. Gudat, W. T. M. Irvine, P. M. Petroff, and D. Bouwmeester, "Strong coupling through optical positioning of a quantum dot in a photonic crystal cavity," *Applied Physics Letters* **94**(11), p. 111115, 2009.
9. A. Laucht, F. Hofbauer, N. Hauke, J. Angele, S. Stobbe, M. Kaniber, G. Böhm, P. Lodahl, M. C. Amann, and J. J. Finley, "Electrical control of spontaneous emission and strong coupling for a single quantum dot," *New Journal of Physics* **11**, p. 023034, 2009.
10. S. Strauf, K. Hennessy, M. T. Rakher, Y.-S. Choi, A. Badolato, L. C. Andreani, E. L. Hu, P. M. Petroff, and D. Bouwmeester, "Self-tuned quantum dot gain in photonic crystal lasers," *Physical Review Letters* **96**(12), p. 127404, 2006.
11. D. Englund, A. Faraon, B. Zhang, Y. Yamamoto, and J. Vučković, "Generation and transfer of single photons on a photonic crystal chip," *Optics Express* **15**, pp. 5550–5558, Apr. 2007.
12. D. Bouwmeester, A. K. Ekert, and A. Zeilinger, eds., *The Physics of Quantum Information, Quantum Cryptography, Quantum Teleportation, Quantum Computation*, Springer, Berlin, 2000.
13. M. A. Nielsen and I. L. Chuang, *Quantum Computation and and Quantum Information*, Cambridge University Press, Cambridge, 2000.
14. A. Laucht, N. Hauke, J. M. Villas-Bôas, F. Hofbauer, G. Böhm, M. Kaniber, and J. J. Finley, "Dephasing of exciton polaritons in photoexcited InGaAs quantum dots in gaas nanocavities," *Physical Review Letters* **103**(8), p. 087405, 2009.
15. A. Faraon, D. Englund, I. Fushman, J. Vučković, N. Stoltz, and P. Petroff, "Local quantum dot tuning on photonic crystal chips," *Applied Physics Letters* **90**(21), p. 213110, 2007.
16. K. Hennessy, A. Badolato, A. Tamboli, P. M. Petroff, E. Hu, M. Atature, J. Dreiser, and A. Imamoglu, "Tuning photonic crystal nanocavity modes by wet chemical digital etching," *Applied Physics Letters* **87**(2), p. 021108, 2005.
17. S. Mosor, J. Hendrickson, B. C. Richards, J. Sweet, G. Khitrova, H. M. Gibbs, T. Yoshie, A. Scherer, O. B. Shchekin, and D. G. Deppe, "Scanning a photonic crystal slab nanocavity by condensation of xenon," *Applied Physics Letters* **87**(14), p. 141105, 2005.
18. S. Strauf, M. T. Rakher, I. Carmeli, K. Hennessy, C. Meier, A. Badolato, M. J. A. DeDood, P. M. Petroff, E. L. Hu, E. G. Gwinn, and D. Bouwmeester, "Frequency control of photonic crystal membrane resonators by monolayer deposition," *Applied Physics Letters* **88**(4), p. 043116, 2006.
19. I. V. Kukushkin, J. H. Smet, L. Hoppel, U. Waizmann, M. Riek, W. Wegscheider, and K. von Klitzing, "Ultrahigh-frequency surface acoustic waves for finite wave-vector spectroscopy of two-dimensional electrons," *Applied Physics Letters* **85**(19), pp. 4526–4528, 2004.
20. M. M. de Lima Jr and P. V. Santos, "Modulation of photonic structures by surface acoustic waves," *Reports on Progress in Physics* **68**(7), pp. 1639–1701, 2005.
21. E. Kuramochi, M. Notomi, S. Mitsugi, A. Shinya, T. Tanabe, and T. Watanabe, "Ultrahigh-q photonic crystal nanocavities realized by the local width modulation of a line defect," *Applied Physics Letters* **88**(4), p. 041112, 2006.
22. J. D. Joannopoulos, S. G. Johnson, J. N. Winn, and R. D. Meade, *Photonic Crystals: Molding the Flow of Light*, Princeton University Press, second ed., 2008.